Research Article

SOHAG JOURNAL OF SCIENCES

https://doi.org/10.21608/sjsci.2025.409045.1301

Adsorptive removal of chromium (VI) ions from solution using P-doped nanostructured carbon materials: Modelling of the adsorption isotherms, Thermodynamics and Kinetic investigation

Omar A.S. Allam[a,b,*], Hatem A. Mahmoud[a], Mervet A. Hamed[b], Kamal M.S. Khalil[a,*]

[a] Chemistry Department, Faculty of Science, Sohag University, Sohag 82524
[b] Environment Department, Soils, Water and Environment Research Institute, Agricultural Research Centre, Giza, Egypt
*[a,b]Email: omarallam@science.sohag.edu.eg
*[a]Email: kms_khalil@science.sohag.edu.eg

Received:30th July 2025 **Revised:** 27th August 2025 **Accepted:** 28th August 2025
Published online: 7th September 2025

Abstract: A series of nanostructured phosphorous P-doped porous carbons synthesized from sorghum stalks biomass were investigated for Cr (VI) adsorptive removal. The adsorbent materials, which were activated at 400, 600 and 800 °C, are characterized by ultra-high surface area (S_{BET}), mesoporous surface area (S_{meso}) and graphene-like structure with slit shaped porosity. The adsorbents showed adsorption capacity, (q_{ads}) in the order of SCP600 > SCP800 > SCP400, which was the same order for total pore volume (V_T), and pore width (P_W). The most active adsorbent, SCP600, showed q_{ads} of 120.1 mg/g at pH of 2. Modeling of the adsorption isotherms were investigated by a group of related isotherms, which showed the best fit with the Langmuir isotherm model. Kinetic of the adsorption process was investigated via three kinetic models and showed to follow the pseudo-second order model. Thermodynamic studies at different initial Cr (VI) concentrations resulted in negative $\Delta H°$, $\Delta S°$, and $\Delta G°$ values. Thus, indicating physicochemical and spontaneous adsorption. The present investigation emphasizes that q_{ads}, of P-doped porous carbon materials derived from sorghum stalks towards Cr (VI) is related not only to S_{BET} and S_{meso} but also to the V_T and P_w SCP of the adsorbent materials.
Keywords: Biomass, type of isotherm, non-leaner fits, ATR_FTIR

1. Introduction

Although industrial development led to easier and more comfortable life for recent generations, the accompanying industrial pollutions by heavy metals have negative impacts on the surrounding environment. Major heavy metals responsible for metal ion pollution include As, Hg, Cu, Ni, Pb, Cr and Cd [1]. Chromium (Cr), which is one of the most hazardous heavy metals in nature, has been extensively employed in many industrial sectors such as electroplating [2], leather tanning [3], wood preservation [4], pigment manufacturing [5] and steel production [6]. There are four valence states for chromium, and the trivalent (Cr^{+3}) and hexavalent (Cr^{+3}) valence states are the most prevalent in aqueous solution. [7]. Moreover, the maximum contamination limit for total Cr in drinking water is 100 µg L^{-1} as stated by the U.S. Environmental Protection Agency [8].

It should be noted that Cr(VI) is 100 times more dangerous than Cr(III) [9]. Since Cr(VI) can cross biological membranes, produce stress, damage the human respiratory system, cause cancer, and be genotoxic, and reproductively harmful [10]. Animals exhibit hematological abnormalities, kidney and liver damage, neurotoxicity, and gastrointestinal distress. Decreased growth, poor photosynthesis, disruption of food intake, oxidative damage, and death are all experienced by plants [9]. Because of its ability to bioaccumulate, it disrupts ecosystems, necessitating effective cleanup methods, regulation, and monitoring to protect human and plant health.

Several researches examined a significant number of common methods for removing chromium from water or wastewater, including precipitation [8], membrane filtration [11], electrolysis [12], extraction [13], adsorption [14], photoreduction [15], and ion exchange [16]. Nevertheless, these traditional methods have included limitations such as high equipment costs, significant energy consumption, and the usage of pricey chemicals. Furthermore, hazardous metals, which might result in secondary pollution, cannot be removed using the above-mentioned conventional processes; [10] and [17]. Conversely, the adsorption has emerged as one of the most common techniques for heavy metal removal due to its effective cost and great efficiency [18]. The conversion of agricultural biomass residue into value added products, such as carbonaceous nanostructured materials, highlights the potential of biomass valorization. Sorghum stalks are under-utilized and little-studied agricultural waste that can be used to produce high-performance carbon materials in a sustainable and affordable manner, which makes the current study economically feasible. Compared to commercial activated carbons, this creative utilization of agricultural biomass produces adsorbent with very good adsorption capability. It

also helps to optimize resources and maintain a sustainable environment instead of burning by farmers.

Porous carbons derived from biomass materials have recently been emphasized as versatile materials as environmental adsorbents for many pollutants [19], [20], [21], [22] and [23], which show high surface area and suitable porosity while they are affordable in almost price less manner. In fact, surface reactivity, surface area, pore size, as well as effective cost are all important considerations when choosing an adsorbent for a particular environmental cleanup application that guarantee peak performance [24]. Recent utilization of biomass-derived activated carbon for chromium removal has been reviewed [25]. The chemical activation methods with KOH and H_3PO_4; which enhance surface area and improve adsorption performance have been emphasized.

Vast number of recent research have utilized porous carbon materials derived from different biomass materials to remove Cr(VI) by adsorption process. This includes, sugar beet [17], orange peel [26], rubber seed shell [27], camellia oleifera shell [18], avocado seed waste [4], in addition carbon nanomaterials such as carbon nanotubes [28], graphene [29], graphene oxide [30].

In the present work, a group of systemically textured P-doped carbon materials, SCP materials, generated from sorghum stalks are investigated as adsorbents for adsorptive removal of Cr(VI) from solutions. Empirical adsorption isotherms as well as the adsorption kinetics were investigated. Moreover, the performance of such adsorbents towards Cr(VI) adsorption was correlated to their surface texture characteristics. Thereby, the optimum surface area and porosity characteristics can be figured out.

2. Materials and methods

2.1. Materials

Phosphoric acid, H_3PO_4 (85%); sodium hydroxide (NaOH, 98%), hydrochloric acid (HCl, 36%) products of Adwic (Egypt), and potassium dichromate, $K_2Cr_2O_7$, (98%), Sigma-Aldrich were employed. Sorghum stalks biomass material was collected from a typical sorghum cereal grain farm in Sohag Government (Egypt) after the harvesting season. Drying was affected naturally leaving the stalks in an open atmosphere.

2.2. Preparation was performed by the method

Preparation was performed as previously described by Khalil et al [31]. Thus, the dried sorghum stalks were impregnated with phosphoric acid, where the acid: sorghum stalk ratio was 2:1 (w/w). The impregnated mixtures were evaporated at 100 °C for 12 h. Then activated at 400, 600, and 800 °C in a flow of N_2 gas (150 mL/min) and heating rate (10 °C /min) for 1 h duration at the target temperature. After cooling down in the flow of N_2, the prepared carbon materials were washed with distilled water until pH of filtrate reached neutral value and then dried for 24 h at 120 °C. The prepared carbon materials, which were activated at 400, 600 and 800 were named SCP400, SCP600 and SCP800, respectively.

2.3. Empirical batch adsorption of Cr(VI)

Chromium Cr(VI) adsorption batch experiments were performed at 25 °C in a thermostatic shaker with an orbital shaking rate of 180 rpm for the specified time intervals. The effect of [initial] of Cr(VI) ions (20–300 mg /L) on adsorption capacity was investigated. Thus, 25 mL of the Cr(VI) solution in a 100 mL bottle flask charged with 50 mg of carbon materials. The initial pH of the solutions was adjusted to pH value of 2.0. After the adsorption equilibrium was attend, concentration of Cr(VI) was determined in the filtered by atomic absorption instrumental method. Thus, the amount adsorbed of Cr(VI), q_e, can be calculated by:

$$q_e = \frac{(C_0 - C_e)V}{W} \quad \ldots\ldots\ldots\ldots\ldots\ldots\ldots\ldots\ldots\ldots\ldots\ldots\ldots\ldots\ldots\ldots (1)$$

where q_e indicates adsorption capacity at equilibrium (mg /g), C_0 and C_e are the initial and equilibrium concentrations of Cr(VI) (mg /L) in the aqueous solution. (V) represents the solution volume, whereas (m) stands for the mass of the adsorbent (g).

Thus, the empirical isotherms of Cr(VI) adsorption on the most active sample were analyzed using four relevant isotherm models of the Langmuir, Freundlich, Temkin as well as the Redlich-Peterson isotherms in their linear forms (Eq. 2-5) and nonlinear form (Eq. 6-9), respectively, as follows:

(i) For linear forms:

$$\frac{C_e}{q_e} = \frac{1}{Q_{max}b} + \frac{1}{Q_{max}}C_e \quad \ldots\ldots\ldots\ldots\ldots\ldots\ldots\ldots\ldots\ldots\ldots\ldots (2)$$

$$logq_e = logK_F + \left(\frac{1}{n}\right) logC_e \quad \ldots\ldots\ldots\ldots\ldots\ldots\ldots\ldots\ldots\ldots (3)$$

$$q_e = B_T \ln K_T + B_T \ln C_e \quad \ldots\ldots\ldots\ldots\ldots\ldots\ldots\ldots\ldots\ldots\ldots\ldots (4)$$

$$\ln\left(\frac{C_e}{q_e}\right) = \beta ln(C_e) - \ln(K_r) \quad \ldots\ldots\ldots\ldots\ldots\ldots\ldots\ldots\ldots\ldots (5)$$

(ii) For nonlinear form:

$$q_e = \frac{q_{max}K_L C_e}{1 + K_l C_e} \quad \ldots\ldots\ldots\ldots\ldots\ldots\ldots\ldots\ldots\ldots\ldots\ldots\ldots\ldots (6)$$

$$q_e = k_f C_e^{\frac{1}{n}} \quad \ldots\ldots\ldots\ldots\ldots\ldots\ldots\ldots\ldots\ldots\ldots\ldots\ldots\ldots\ldots\ldots (7)$$

$$q_e = B \ln AC_e \quad \ldots\ldots\ldots\ldots\ldots\ldots\ldots\ldots\ldots\ldots\ldots\ldots\ldots\ldots\ldots\ldots (8)$$

$$q_e = \frac{A_{RP}C_e}{1 + B_{RP}C_e^{\beta}} \quad \ldots\ldots\ldots\ldots\ldots\ldots\ldots\ldots\ldots\ldots\ldots\ldots\ldots\ldots\ldots (9)$$

where, q_e (mg/g) represents equilibrium adsorption capacity, and b (L/mg), K_F, K_T and K_r are Langmuir, Freundlich, Temkin and Redlich-Peterson isotherm constant, respectively. β is dimensionless Redlich-Peterson exponent.

The dimensionless separation factor (R_L), defined by Eq (10), was employed whenever the Langmuir isotherm was applicable.

$$R_L = \frac{1}{1 + bC_0} \dots\dots\dots\dots\dots\dots\dots\dots\dots\dots\dots (10)$$

Where C_0 and K_L stand for the Cr(VI) initial concentration (mg/L) and Langmuir constant, respectively. The four types of adsorptions behaviors can be indicated based of R_L value as (i) unfavorable ($R_L > 1$), (ii) linear ($R_L = 1$), (iii) irreversible ($R_L = 0$), and (iv) favorable ($0 < R_L < 1$).

2.4. Thermodynamics and kinetics investigation

The adsorption rate at different initial concentration of Cr(VI) ions (50–200 mg /L) on adsorption capacity for the most active sample was investigated. Thus, the equilibrium concentrations (q_t) at different time intervals (t) were determined via (Eq.1) to construct the adsorption rate curves.

The kinetics of the adsorption process were investigated in terms of different kinetic models. This involves the pseudo-first-order model (Eq. 11), the pseudo-second-order model (Eq. 12), and the intra-particle-diffusion model (Eq. 13)

$$ln(q_e - q_t) = lnq_e - k_1 t \dots\dots\dots\dots\dots\dots\dots\dots\dots\dots\dots (11)$$

$$\frac{t}{q_t} = \frac{1}{k_2 q_e^2} + \frac{t}{q_e} \dots\dots\dots\dots\dots\dots\dots\dots\dots\dots\dots (12)$$

$$q_t = q_{int} t^{1/2} + C \dots\dots\dots\dots\dots\dots\dots\dots\dots\dots\dots (13)$$

Where q_t and q_e represent the amounts of Cr(VI) adsorbed (mg/g) at time (t, min) and at equilibrium, respectively. Whereas k_1 (min^{-1}), and k_2 ($g.mg^{-1}$ min^{-1}) represent respectively, the rate constants for the pseudo–first-order and pseudo–second order models.

The effect of adsorption temperature was studied in the range of (25–40 ºC) at [initial] concentration of 100 and 300 mg/L on the SCP600 material. The Gibbs free energy change ($\Delta G°$), enthalpy change ($\Delta H°$), and entropy change ($\Delta S°$) were calculated from (Eq. 14), and (Eq. 15),

$$LnK_c = \frac{\Delta S°}{R} - \frac{\Delta H°}{R}\left(\frac{1}{T}\right) \dots\dots\dots\dots\dots\dots\dots\dots\dots\dots\dots (14)$$

$$\Delta G° = \Delta H - T\Delta S° \dots\dots\dots\dots\dots\dots\dots\dots\dots\dots\dots\dots (15)$$

Where R is the universal gas constant and K_C is the equilibrium constant.

3. Results and Discussion:

3.1. Characteristics of adsorbent materials

Texture and structure of porous carbon derived from sorghum stalks by H_3PO_4 were thoroughly investigated [31]. The main textural characteristics of the current test materials, SCP400, SCP600 and SCP800, are cited in Table 1, which shows the main surface textural characteristics of the materials in terms of specific surface area (S_{BET}); external surface area (S_{Ext}); mesoporosity percentage S_{meso}% (S_{Ext}/S_{BET}) ×100, total pore volume (V_T), and pore width (Pw) by the BJH method, respectively.

Thus, high surface area values amount to (2083, 2228, and 2443 m^2/g) were observed for the adsorbent materials SCP400, SCP600 and SCP800, respectively. Moreover, S_{Ext} increase ($1717 < 2203 < 2443$ m^2/g) and S_{micro} decrease ($366 > 24 > 0$ m^2/g) in the direction the activation temperature increase (SCP400, SCP600 and SCP800). This resulted in S_{meso} percentages values amount (82.4, 98.9, and 100) for SCP400, SCP600 and SCP800, respectively. However, V_T values amount to (1.494, 1.792 and 1.651 cm^3 /g) and P_w (BJH) amounts to (38.1, 43.7 and 35.2 Å) for SCP400, SCP600 and SCP800, respectively, were observed.

Table 1. Surface Texture characteristics for the test materials SCP400, SCP600 and SCP800.

Sample Name	S_{BET} (m^2/g)	S_{Ext} (m^2/g)	S_{micro} (m^2/g)	S_{meso} %	V_T (cm^3 /g)	P_w (BJH) (Å)
SCP400	2083	1716	366	82.4	1.494	38.1
SCP600	2228	2203	24	98.9	1.792	43.7
SCP800	2443	2443	0	100	1.651	35.2

$V_T = cm^3/g$ was measured at $p/po = 0.97$
$S_{meso}\% = S_{Ext}/S_{BET} \times 100$

3.2. Adsorption isotherms for Cr(VI) ions

The empirical Cr(VI) adsorption curves on SCP400, SCP600 and SCP800 group of adsorbent materials at 25°C are presented in Fig. 1. Thus, the isotherms indicated effective adsorptions for all the samples. Thus, at low equilibrium concentration, $q_e < 30$ mg/L the order of adsorption is SCP600 > SCP400 > SCP800. Whereas at higher q_e values (> 30 mg/L), the order changed into SCP600 > SCP800 > SCP400. Therefore, SCP600 was considered the most active sample.

3.3. Modeling of adsorption isotherms

Modeling of the empirical data was investigated by linear and non-linear fits of the chosen isotherm models, Eq. 2-5, and Eq. 6-9, respectively. The results were presented for linear (Fig. 2) and nonlinear (Fig. 3) fits, respectively.

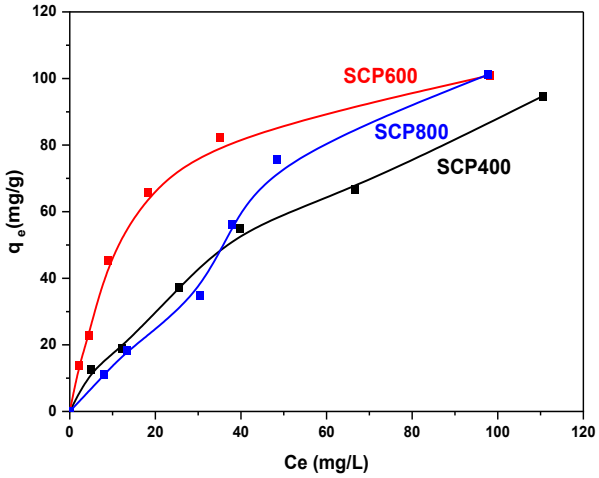

Fig. 1. Adsorption isotherm of Cr(VI) on SCP400, SCP600 and SCP800 adsorbents as indicated.

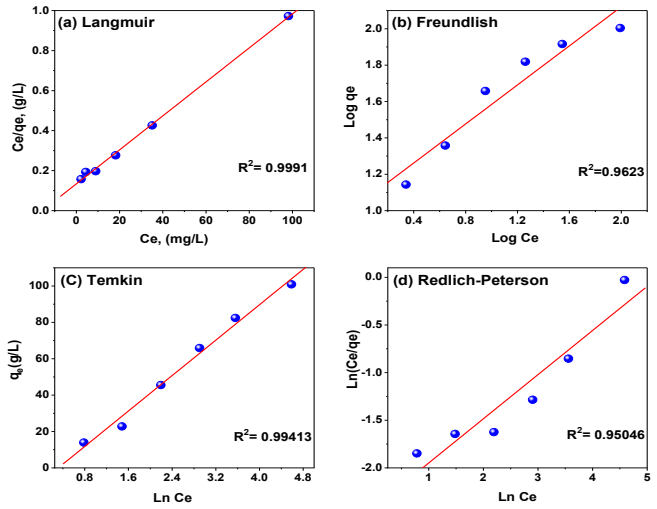

Fig. 2. The linear fits for the Langmuir, Freundlich, Temkin and Redlich-Peterson isotherm of Cr(VI) adsorption on SCP600 adsorbent.

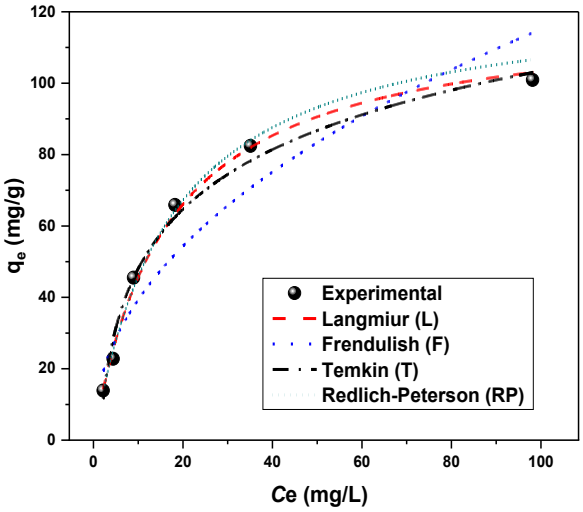

Fig. 3. The nonlinear fits for the Langmuir, Freundlich, Temkin and Redlich-Peterson isotherm of Cr(VI) adsorption on SCP600 adsorbent

Moreover, the corresponding fit parameters were cited for linear (Table 2 A) and nonlinear (Table 2 B), respectively. Both linear and non-linear fits indicated the applicability of the Langmuir adsorption model (from R^2 and other parameters).

Considering the Langmuir model, R_L value was calculated, which equals 0.016. This value indicates the favorable nature of the adsorption process on SCP600.

3.4. Adsorption Kinetics

The rate of the adsorption process was investigated over the most active sample at different initial Cr(VI) concentrations (50–200 mg/L), Fig. 4. Modeling of the rate curves was investigated through the chosen models on SCP600. The fit results were represented in Fig. 5, whereas the fit parameters were listed in Table S1. The results show that the Cr(VI) adsorption process follows the pseudo-second order model Fig. 5 (B). However, no applicability for the other models were observed, Fig. 5 (A and C), respectively

3.5. Adsorption Thermodynamics

The adsorption process thermodynamics for Cr(VI) on SCP600 was investigated at different temperatures (298, 302, 308 and 313 K) at two different Cr(VI) ions concentrations (100 and 300 mg/L). The standard thermodynamic parameters ($\Delta H°$, $\Delta S°$, and $\Delta G°$) were calculated using Eqs. (14) and (15), the calculated thermodynamic parameters on SCP600 were listed in Table 3. Considering the negative values obtained for $\Delta H°$ (–3.82 and – 4.98 kJ/mol at Cr(VI) concentrations 100 and 300 mg/L) indicates the process exothermic nature, which confirm its adsorptive nature. Moreover, the resulted, ΔS values (–1.87 and – 4.68 J/mol K) indicate that the adsorption process on SCP600 reduces the randomness at solvent–liquid interface [27], as reflected from the negative value of ΔS. The calculated $\Delta G°$, which amounts to, –2.41 and –4.36 kJ/mol for 100 and 300 mg/L, respectively, indicates a spontaneous nature of the adsorption.

Table 2. (A) The liner fits parameters for the different adsorption models examined on the most active adsorbent.

Langmuir isotherm				Freundlich isotherm		
Q_{max} mg/g	b (L/mg)	R^2	R_L	K_F	1/n	R^2
117.6	0.0634	0.999	0.016	11.1509	0.637	0.962
Temkin isotherm			**Redlich-Peterson**			
B	K_T	R^2		K_r	β	R^2
24.343	0.729	0.994		11.1507	0.463	0.950

Table 2. (B) The non-liner fits parameters for the different adsorption models examined on the most active adsorbent.

Langmuir isotherm			Freundlich isotherm		
Q_{max} mg/g	b (L/mg)	R^2	K_F	1/n	R^2
120.1	0.061	0.995	13.49	0.465	0.915
Temkin isotherm			**Redlich-Peterson**		
B	K_T	R^2	K_r	β	R^2
24.024	0.741	0.983	7.297	0.999	0.993

Table 3. The thermodynamics parameters for Cr(VI) adsorption process on SCP600 at different temperature 25–40 °C (298–313K).

Concentration (mg/L)	$\Delta H°$ kJ/mol	$\Delta S°$ J/molK^{-1}	$\Delta G°$, kJ/mol			
			298 K	303 K	308 K	313 K
100	-3.815	-4.68	-2.41	-2.38	-2.36	-2.34
300	-4.98	-1.87	-4.423	-4.413	-4.404	-4.395

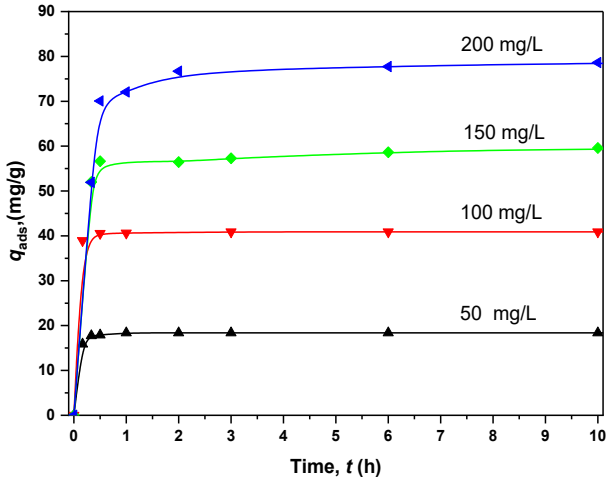

Fig. 4. Effects of contact time at different initial concentrations on the adsorption capacity of Cr(VI) on SCP600 adsorbent as indicated.

3.6. Characteristics of the spent adsorbent

ATR–FTIR spectra of adsorbent before and after the adsorption process was investigated by ATR–FTIR, Fig. 6. Moreover, Table 4 lists the bands that were observed and their assignments in light of some recently published works [27], [32], [33] and [34].

A comparison between the present materials, some other recently reported adsorbents was presented in Table 5. This demonstrates that the produced SCP600 adsorbent materials exhibited exceptional high adsorption capacity up to 120.1 mg/g

Table 4. FTIR-ATR bands assignments for the SCP600 adsorbent material before and after adsorption of Cr(VI).

Wave number cm^{-1}	Assignment	Effect of Cr (VI) adsorption	References
1700	ν C═O carboxylic acid	increase	[35]
1565	ν (C═C) aromatic ring stretching	increase	[34]
1455	δ(O–H) of phenol type surface group	decrease	[36]
1192	assigned for ν (C–O)	decrease	[31]
1167	H-bonded ν(P═O), or ν(O–C) in P− O− C (aromatic) and ν(O═P–OH)	decrease	[37]
1065	ν (P–O–C) acidic phosphate esters, ν_s (P–O–P) chain	decrease	[38]
880	Cr═O	appeared	[39]
480	δ modes of the phosphate ion	decrease	[32]

Table 5. Comparison between the Cr(VI) adsorption capacity of some recent published adsorbents with the present SCP600

Raw materials	Activation agent	Maximum adsorption capacity (mg/g)	References
longan seed	NaOH	35.02	[40]
mango kernel	H_3PO_4	7.8	[41]
sawdust	$ZnCl_2$	13.15	[42]
nutshell	H_3PO_4	74.9	[43]
apple peels	NaOH	36.01	[44]
Corn stalk	KOH	89.5	[45]
Eucalyptuscamadulensis seeds	H_3PO_4	51.9	[46]
Sorghum stalks	H_3PO_4	120.1	This study

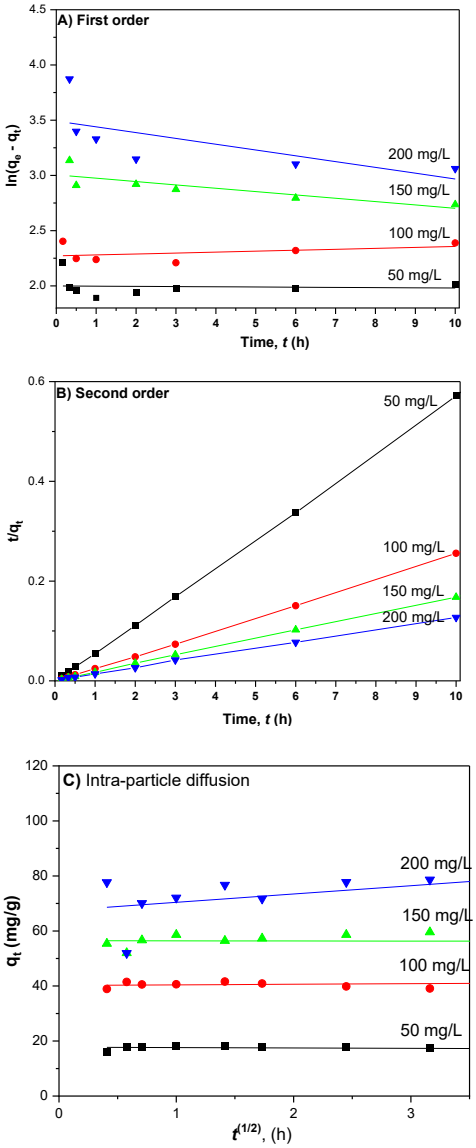

Fig. 5. Adsorption rate fits with pseudo-first order (A), pseudo-second order (B) and intra-particle diffusion (C) plots for the adsorption of Cr(VI) adsorption on SCP600 adsorbent.

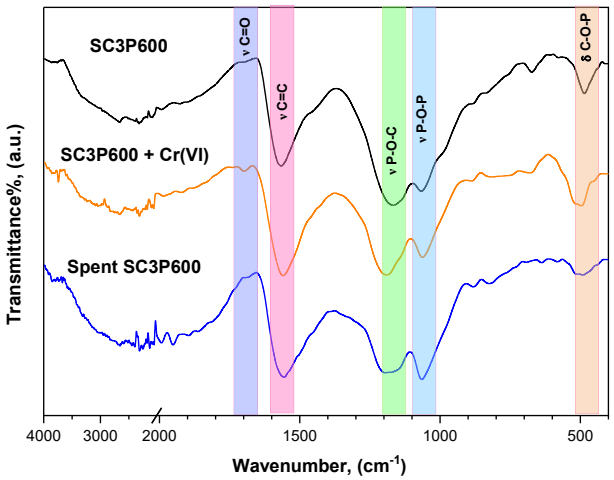

Fig. 6. ATR-FTIR spectra of SCP600 adsorbent before and after Cr(VI) adsorption.

3.7. Adsorption Mechanism of Cr (VI)

After the adsorption of Cr(VI), the FTIR-ATR spectra for SCP600 revealed the presence of several oxygen-containing functional groups, including hydroxyl, phenolic, and phosphate. The phosphate related groups (C-O-PO3) were mainly responsible for the adsorption of chromium(VI) ions, by ion exchange or electrostatic attraction. Furthermore, the diffusion of Cr(VI) across a plate-like mesoporous structure facilitated the physical adsorption between SCP600 adsorbent and Cr(VI) ions . A pH of 2.0 should cause the SCP600 adsorbent's surface to become protonated, with the majority of the Cr(VI) ions present as $HCrO4^{-}$ and $Cr2O7^{2-}$ oxo-anions. Strong electrostatic interaction between the negatively charged Cr(VI) oxo-anions and the positively charged functional groups of the adsorbent was caused by the large amount of protonation anticipated for the P-related active sites at pH value of 2. Additionally, the high redox potential range of 1.33–1.38 V in this case might readily result in the reduction of Cr (VI) to Cr (III) [21].

4. Conclusion

The P–doped porous carbon materials produced from sorghum stalks showed an exceptional capacity to remove Cr(VI), with a maximum Langmuir adsorption capacity of 120.1 mg/g. The adsorption isotherms are compatible with the Langmuir isotherm and the pseudo-second order kinetics. In conclusion, porous carbon materials derived from sorghum stalks can be regarded as efficient adsorbent. This in fact emphasizes the immense value of the biomass-derived porous materials as an adsorbent for Cr(VI) ion. The success of this utilization will help the valorization of sorghum stalks biomass residues and prevent biomass burning by the farmer. The overall work, which involves the environmental process for carbon sequestration and its subsequent application for an environmental contaminant removal process will support environmental remediation protection and preservation.

CRediT authorship contribution statement:

Kamal M.S. Khalil: Writing – review & editing, Supervision, Methodology, Conceptualization, Formal analysis, Funding acquisition, Resources, Validation, Visualization. Omar A.S. Allam: Writing – original draft, Investigation, Formal analysis, data curation, Conceptualization, Methodology, Software. Hatem A. Mahmoud: Supervision, Software, Investigation, Conceptualization, Data curation, Formal analysis, Writing – original draft, Methodology. Mervet A. Hamed: Visualization, Supervision, Investigation, Conceptualization, Methodology, Validation. All authors have read and agreed to the published version of the manuscript.

Data availability statement

The data used to support the findings of this study are available from the corresponding author upon request.

Declaration of Competing Interest

The authors declare that they have no known competing financial interests or personal relationships that could have appeared to influence the work reported in this paper.

References

[1] P.B. Angon, M.S. Islam, S. KC, A. Das, N. Anjum, A. Poudel, S.A. Suchi, *Heliyon,* 10 (2024) e28357.

[2] A. Husain, S. Ayub, A.H. Khan, S.S. Alam, M.A. Hasan, *Environmental Management*, 391 (2025) 126502.

[3] Y.G. Wibowo, D. Anwar, H. Safitri, A. Setiawan, S. Sudibyo, A.T. Yuliansyah, H.T.B. Murti Petrus, *Colloids Surfaces C Environ. Asp*., 3 (2025) 100066.

[4] K. Mabalane, N.D. Shooto, P.M. Thabede, P.M. Thabede, *Chem. Environ. Eng*., 10 (2024) 100782.

[5] S. Ganguly, S. Ganguly, *Results Eng*. (2025) 106246.

[6] M. Abewaa, A. Arka, T. Haddis, A. Mengistu, T. Takele, E. Adino, Y. Abay, N. Bekele, G. Andualem, H. Girmay, *Results Eng.,* 22 (2024) 102274.

[7] Z.A. AL-Othman, Ali, R., M. Naushad, *Chem. Eng. J*., 184 (2012) 238–247.

[8] C. Wu, J. Zhou, S. Pang, L. Yang, E. Lichtfouse, H. Liu, S. Xia, B.E. Rittmann, *Water Res.,* 249 (2024) 120878.

[9] S. Shirazian, T. Huynh, N. Pirestani, R. Soltani, A. Marjani, A.B. Albadarin, S.M. Sarkar, *J. Colloid Interface Sci.,* 664 (2024) 667–680.

[10] M. Tan, S. Yang, C. Song, Z. He, J. Wang, Y. Liu, F. Liu, Y. Zhang, *Chem. Eng. J.,* 499 (2024) 156182.

[11] H. Peng, J. Guo, *Environ. Chem. Lett*., 18 (2020) 2055–2068.

[12] F.A. Soriano Moranchell, J.M. Sandoval Pineda, J.N. Hernández Pérez, U.S. Silva-Rivera, C.A. Cortes Escobedo, R. de G. González Huerta, *Int. J. Hydrogen Energy,* 45 (2020) 13683–13692.

[13] Y. Jia, Y. Qing, B. Feng, Y. Zhong, L. Dai, M. Wang, *Purif. Technol*., 343 (2024) 127098.

[14] T. Shao, Q. Yin, J. Bai, J. Zhu, M. Gan, *Environ. Res.,* 266 (2025) 120449.

[15] D.V. Wellia, R.M. Rahma, S. Arief, R. Subagyo, Y. Kusumawati,. *Chem. Environ. Eng*., 9 (2024) 100719.

[16] P. Thiripelu, J. Manjunathan, M. Revathi, P. Ramasamy, *J. Water Process Eng*., 58 (2024) 104815.

[17] J. Zhao, L. Yu, F. Zhou, H. Ma, K. Yang, G. Wu, *RSC Adv*., 11 (2021) 8025–8032.

[18] Z. Zheng, H. Zhao, X. Lin, J. Yang, R. Shi, *Desalin. Water Treat*., 198 (2020) 170–179.

[19] K.M.S. Khalil, O.A.S. Allam, M. Khairy, K.M.H. Mohammed, R.M. Elkhatib, M.A. Hamed, *J. Mol. Liq*., 247 (2017) 386–396.

[20] Y. Son, Neelam, P.C. Rao, J. Lee, M. Yoon, *J. Environ. Chem. Eng.,* (2025) 118036.

[21] K.M.S. Khalil, W. Elhamdy A., K.M.H. Mohammed, A.E.A.A. Said, *Mater*. *Chem. Phys*., 282 (2022) 125881.

[22] K.M.S. Khalil, W.A. Elhamdy, A.E.A.A. Said, *Int. J. Hydrogen Energy,* 51 (2024) 819–833.

[23] K. Kumar, R. Kumar, S. Kaushal, N. Thakur, A. Umar, S. Akbar, A.A. Ibrahim, S. Baskoutas, *Chemosphere,* 345 (2023) 140419.

[24] P. Kaur, S. Kumar, J. Rani, Jn. Babu, S. Mittal, *Environ. Sci. Pollut. Res.,* 31 (2024) 52371–52390.

[25] N.R. Putra, M.A.A. Zaini, H.S. Kusuma, H. Darmokoesoemo, A.N.M. Faizal, *Environ. Prog. Sustain. Energy,* 44 (2025) e14598.

[26] K.M.S. Khalil, W.A. Elhamdy, A.A. Elsamahy, *Colloids Surfaces A Physicochem. Eng*. Asp. 641 (2022) 128553.

[27] P. Kongsak, T. Supattra, T. Suphawarat, *Desalin*. *Water Treat*., 313 (2023) 173–185.

[28] Ihsanullah, F.A. Al-Khaldi, B. Abu-Sharkh, A.M. Abulkibash, M.I. Qureshi, T. Laoui, M.A. Atieh, *Desalin*. *Water Treat.* 57 (2016) 7232–7244.

[29] N. Ngainunsiami, L. Lalhmunsiama, A. Tiwari, R. Diwakar, *Chem. Eng. Res. Des*., 219 (2025) 67–78.

[30] C.D. Ghugare, N. V. Rathod, J.S. Jadhao, A. Rao, A.V. Kubade, P.S. Thakare, A.B. Patil, *Chem. Inorg. Mater*., 6 (2025) 100105.

[31] K.M.S. Khalil, O.A.S. Allam, H.A. Mahmoud, M.A. Hamed, *Int. J. Biol. Macromol*., 307 (2025) 141736.

[32] M. Myglovets, O.I. Poddubnaya, O. Sevastyanova, M.E. Lindström, B. Gawdzik, M. Sobiesiak, M.M. Tsyba, V.I. Sapsay, D.O. Klymchuk, A.M. Puziy, *Carbon N. Y*., 80 (2014) 771–783.

[33] E. Fuente, J.A. Menéndez, M.A. Díez, D. Suárez, M.A. Montes-Morán, *J. Phys. Chem. B*, 107 (2003) 6350–6359.

[34] H. Zeng, H. Zeng, H. Zhang, A. Shahab, K. Zhang, Y. Lu, I. Nabi, F. Naseem, H. Ullah, *J. Clean. Prod.,*. 286 (2021) 124964.

[35] K. Huang, S. Yang, X. Liu, C. Zhu, F. Qi, K. Wang, J. Wang, Q. Wang, T. Wang, P. Ma, *J. Clean. Prod*., 391 (2023) 136174.

[36] J. Coates, *Encycl. Anal. Chem*., (2000) 10815–10837.

[37] A.M. Puziy, O.I. Poddubnaya, A. Martínez-Alonso, A. Castro-Muñiz, F. Suárez-García, J.M.D. Tascón, *Carbon N. Y.*, 45 (2007) 1941–1950.

[38] A.M. Puziy, O.I. Poddubnaya, A. Martínez-Alonso, F. Suárez-García, J.M.D. Tascón, *Carbon N. Y.,* 43 (2005) 2857–2868.

[39] K. Rambabu, F. Banat, G.S. Nirmala, S. Velu, P. Monash, G. Arthanareeswaran, Desalin. *Water Treat*., 156 (2019) 267–277.

[40] J. Yang, M. Yu, Chen, Wentao, *J. Ind. Eng. Chem*., 21 (2015) 414–422.

[41] M.K. Rai, G. Shahi, V. Meena, R. Meena, S. Chakraborty, R.S. Singh, B.N. Rai, *Resour. Technol*., 2 (2016) S63–S70.

[42] C. Chen, P. Zhao, Z. Li, Z. Tong, *Desalin. Water Treat*., 57 (2016) 12572–12584.

[43] A. Kumar, H.M. Jena, *J. Environ. Chem., Eng.* 5 (2017) 2032–2041.

[44] I. Enniya, L. Rghioui, A. Jourani, *Chem. Pharm*., 7 (2018) 9–16.

[45] J. Zhao, L. Yu, H. Ma, F. Zhou, K. Yang, G. Wu, *J. Colloid Interface Sci*., 578 (2020) 650–659.

[46] E. Suganya, N. Saranya, S. Sivaprakasam, L.A. Varghese, S. Narayanasamy, *Environ. Technol. Innov*., 19 (2020) 100977.